



An efficient multi-objective optimization method based on the adaptive approximation model of the radial basis function

Xin Liu^{1,2} · Xiang Liu² · Zhenhua Zhou² · Lin Hu²

Received: 18 May 2020 / Revised: 21 September 2020 / Accepted: 9 October 2020 / Published online: 31 October 2020
© Springer-Verlag GmbH Germany, part of Springer Nature 2020

Abstract

Considering the high computational cost caused by solving multi-objective optimization (MOO) problems, an efficient multi-objective optimization method based on the adaptive approximation model is developed. Firstly, the Latin hypercube design (LHD) is employed for obtaining the initial sample points. Secondly, initial approximation models of objective functions and constraints are established by using the radial basis function (RBF). For ensuring the accuracy of the approximation models, the reverse shape parameter analysis method (RSPAM) is proposed to obtain improved approximation models. Thirdly, the micro multi-objective genetic algorithm (μ MOGA) is adopted to solve the Pareto optimal set and the local-densifying approximation method is also applied to strengthen the ability of solving accurate Pareto optimal sets. Finally, the effectiveness and practicability of the proposed method is demonstrated by two numerical examples and two engineering examples.

Keywords Multi-objective optimization · Reverse shape parameter analysis method · Local-densifying approximation method · Adaptive approximation model

1 Introduction

The multi-objective optimization (MOO) problems widely exist in engineering design (Zarchi and Attaran 2019; Tian et al. 2018; Wang et al. 2011; Jaouadi et al. 2020), and a large number of optimization schemes have been provided by different MOO methods. A series of prominent work in this filed has been carried out and reported. Omkar et al. (2011) proposed a vector evaluated artificial bee colony (VEABC) algorithm to deal with the multi-objective design optimization of the laminated composite components. Bui et al. (2019) suggested a multi-objective optimization method based on the mixed integer linear programming (MILP) to determine

trade-off between conflicting operation objectives of wind farm systems. Posteljnik et al. (2016) proposed a multi-objective optimization method for the wind turbine structure by adopting the particle swarm (PSO) algorithm. In the abovementioned works, the multi-objective optimization problems are mostly formulated by explicit mathematical expressions. However, the objective functions and constraints are usually black-box functions for most MOO problems, which are evaluated by complex simulation model with high computational costs and poor efficiency (Liu et al. 2015, 2017a, b; Hu et al. 2020). Therefore, an efficient method for solving the MOO problems should be developed.

To achieve better efficiency of the existing MOO method in dealing with the complex engineering problems, many scholars use the approximation model instead of the actual numerical simulation model such as Kriging (Choi et al. 2018), radial basis function (RBF) (Liew et al. 2004), and support vector regression (Lu and Roychowdhury 2008). Furthermore, a series of optimization methods based on the approximation model are further developed, which are extensively utilized in the optimal design of complex engineering problems. Kiani and Yildiz (2016) adopted the radial basis function to optimize the crashworthiness and NVH of the vehicle. Bu et al. (2018) employed the adaptive Kriging model to optimize the physical properties of the flywheel motor.

Responsible Editor: Ren-Jye Yang

✉ Zhenhua Zhou
liuxinzhenghua@163.com

¹ Engineering Research Center of Catastrophic Prophylaxis and Treatment of Road & Traffic Safety of Ministry of Education, Changsha University of Science & Technology, Changsha 410114, China

² Hunan Province Key Laboratory of Safety Design and Reliability Technology for Engineering Vehicle, Changsha University of Science and Technology, Changsha 410114, China

Manshadi and Jamalinasab (2017) used response surface model to optimize the flap shape of unmanned aerial vehicle. In the reliability analysis (Liu et al. 2019a, 2020; Peng et al. 2018), the approximation model is also commonly used. Liu et al. (2019b) applied the radial basis function to perform the reliability analysis of complex structures. Zhang et al. (2017) adopted the response surface to evaluate the time-dependent reliability of uncertain structures. In order to further improve the accuracy of multi-objective optimization algorithm, the adaptive approximation model which contains updating management frameworks is also employed for the MOO problems. Yang et al. (2002) solved the multi-objective optimization problem of the I-beam structure by adopting the adaptive approximation models which are sequentially updated during the iterative optimization process. Fang et al. (2014) employed the multi-objective particle swarm optimization (MOPSO) algorithm for the crashworthiness design by using the adaptive approximation models, in which sequential sampling points are generated over the design space and the Kriging models are refitted in an iterative fashion. Jang et al. (2009) proposed an adaptive approximation framework and a convergence criterion of the adaptive approximation model to perform the multi-objective optimization for the full stochastic fatigue design problem. In the above works, the approximation model is widely used to solve engineering problems, but it is only the engineering application of approximation model and the method of constructing approximation model is not detailed discussed. Considering the accuracy of approximation model directly affects the optimization results of engineering problems, hence the method of constructing approximation model should be further researched.

In recent years, many studies have been proposed on how to achieve better efficiency and accuracy of the approximation models. Wang et al. (Wang et al. 2001; Wang 2003) developed the inherited Latin hypercube sampling (LHS) approach to strengthen the prediction ability and stability of the adaptive response surface. Cheng et al. (2015) proposed a trust region peak tracking sampling approach to enhance the ability of approximation model when dealing with the high-dimensional problems. Garud et al. (2017) suggested a united sampling criterion to enhance the overall accuracy of the global optimum in the approximation-based problems. As mentioned above works, the accuracy of approximation model is improved effectively based on the selection and layout of samples. It is noteworthy that the shape parameters of the approximation model, nonlinearity of objective functions, and constraints also affect the accuracy of the approximation model besides the samples. Although some scholars (Stolbunov and Nair 2018; Fasshauer and Zhang 2007; Long et al. 2016; Lee et al. 2008; Koupaei et al. 2018; Sarra and Sturgill 2009; Fornberg and Piret 2008) have studied the selection methods of the shape parameters in the constructing approximation model process, these methods determine the

shape parameters by samples and use the same shape parameters to construct approximation models of different nonlinear optimization objective functions and constraints, which will inevitably cause the error of approximation model. Considering the existence of different nonlinear optimization objective functions and constraints, therefore, the shape parameters should be determined according to specific optimization objective functions and constraints rather than only according to samples. Meanwhile, the prediction ability of the approximation model cannot be guaranteed by the construction of the primary approximation model. Therefore, further studies for updating approximation model are necessary. This method should determine the location and direction of the distribution samples through the model management technology, so as to continuously update the samples and modify the approximation model until the accuracy requirements are reached. Hence, for promoting the MOO method into practical applications, the high-efficiency MOO methods with approximation model need to be developed.

For the above reasons, an efficient MOO method based on the adaptive approximation model is developed and applied to the practical engineering applications in this paper. The frame of this paper is organized as follows: the MOO problem and the related definitions are first introduced in Section 2. Then, an efficient MOO method based on the adaptive approximation model is detailed and discussed in Section 3. In Section 4, two numerical examples and two engineering examples are investigated to demonstrate the effectiveness of the present method. Finally, some conclusions are summarized in Section 5.

2 Statement of the multi-objective optimization problem

A typical description of multi-objective optimization (MOO) problem is as follows:

$$\begin{aligned} \min_{\mathbf{X}} f_i(\mathbf{X}), \quad & i = 1, 2, \dots, a \\ \text{s.t. } h_u(\mathbf{X}) = 0, \quad & u = 1, \dots, b \\ g_v(\mathbf{X}) \leq 0, \quad & v = 1, \dots, c \\ \mathbf{X} = (X_1, X_d, \dots, X_n)^T, \quad & d = 1, \dots, n \end{aligned} \quad (1)$$

where $\mathbf{X} = (X_1, X_d, \dots, X_n)^T$ stands for the n -dimensional vector which consists of design variables. $f_i(\mathbf{X})$ denotes the objective function. $h_u(\mathbf{X})$ and $g_v(\mathbf{X})$ represent the equality constraint and the inequality constraint, respectively. During the process of solving the abovementioned multi-objective problems, a series of feasible solutions can be solved. \mathbf{X}_ξ and \mathbf{X}_ψ are individual solutions in the feasible set Ω_S , namely, $\mathbf{X}_\xi, \mathbf{X}_\psi \in \Omega_S$. If the objectives corresponding to the solution \mathbf{X}_ξ are partially superior to the objectives corresponding to the

Table 1 Different basis functions

No.	Name	Basis function	Shape parameter
1	Gaussian	$e^{-\varepsilon r^2}$	ε
2	Cubic	$(r^2 + \varepsilon)^3$	ε
3	Inverse multiquadric	$(r^2 + \varepsilon^2)^{-\frac{1}{2}}$	ε
4	Logistic	$1/(1 + e^{\varepsilon r})$	ε

solution \mathbf{X}_{ψ} , it is defined that the solution \mathbf{X}_{ξ} dominates the solution \mathbf{X}_{ψ} , written as $\mathbf{X}_{\xi} \prec \mathbf{X}_{\psi}$. If the objectives corresponding to the solution \mathbf{X}_{ξ} are all superior to the objectives corresponding to the solution \mathbf{X}_{ψ} , it is defined that the solution \mathbf{X}_{ξ} strongly dominates the solution \mathbf{X}_{ψ} , written as $\mathbf{X}_{\xi} \prec \mathbf{X}_{\psi}$. If $\mathbf{X}^* \in \Omega_S$ and there is no $\mathbf{X} \in \Omega_S$ dominating \mathbf{X}^* , the solution \mathbf{X}^* is defined as the Pareto optimal solution or non-dominated solution of the multi-objective optimization problem.

The Pareto optimal solutions in the feasible set Ω_S are considered to be equally important unless further information is provided from the decision-maker. These Pareto optimal solutions are defined as the Pareto optimal set or non-dominated set. The Pareto optimal set converge into a curve in the feasible design space which is defined as the Pareto optimal frontier. The aim of the multi-objective optimization algorithm is to find the Pareto optimal set to form the Pareto frontier. However, the challenge to the most MOO problems is that the objective functions and constraints are usually implicitly functions, which are evaluated by complex simulation model with high computational costs and low efficiency. Therefore, a multi-objective optimization method with high efficiency should be developed.

3 The multi-objective optimization method based on the adaptive approximation model

As mentioned above, during the process of solving multi-objective optimization problems, complex function evaluations may cause a high computational cost and low efficiency. Thus, an efficient MOO method based on the adaptive approximation model will be developed and discussed in the following contents.

3.1 Radial basis function (RBF)

Radial basis function is a linear combination of radial functions with respect to the Euclidean distance between the predict points and the sample points (Amouzgar and Strömberg 2017; Zhang et al. 2020), which can be used to approximate complex simulation model or black-box function. The RBF can be defined as:

$$\tilde{f}(\mathbf{X}) = \sum_{i=1}^N w_i h(r_i) \tag{2}$$

where $\tilde{f}(\mathbf{X})$ denotes the response value of approximate function. N is the number of samples which are generated by the experimental design such as the Latin hypercube design (LHD) (Park 1994; Joseph et al. 2015; Husslage et al. 2011). w_i represents the coefficient of the linear combinations. $h(r_i)$ is the basis function, and $r_i = \|\mathbf{X} - \mathbf{X}_i\|$ is the Euclidean distance between the predict point and the samples.

When N samples are obtained, the corresponding RBF model can be expressed as:

$$\mathbf{f} = \mathbf{h}\mathbf{w} \tag{3}$$

where \mathbf{f} denotes the N -dimensional response vector of samples. \mathbf{w} is the coefficient vector. \mathbf{h} represents $N \times N$ dimensional matrix, which is described as follows:

$$\mathbf{h} = \begin{pmatrix} h(\|\mathbf{X}_1 - \mathbf{X}_1\|) & \cdots & h(\|\mathbf{X}_1 - \mathbf{X}_N\|) \\ \vdots & \ddots & \vdots \\ h(\|\mathbf{X}_N - \mathbf{X}_1\|) & \cdots & h(\|\mathbf{X}_N - \mathbf{X}_N\|) \end{pmatrix} \tag{4}$$

And the coefficient vector \mathbf{w} can be calculated by Eq. (5):

$$\mathbf{w} = \mathbf{h}^{-1} \mathbf{f} \tag{5}$$

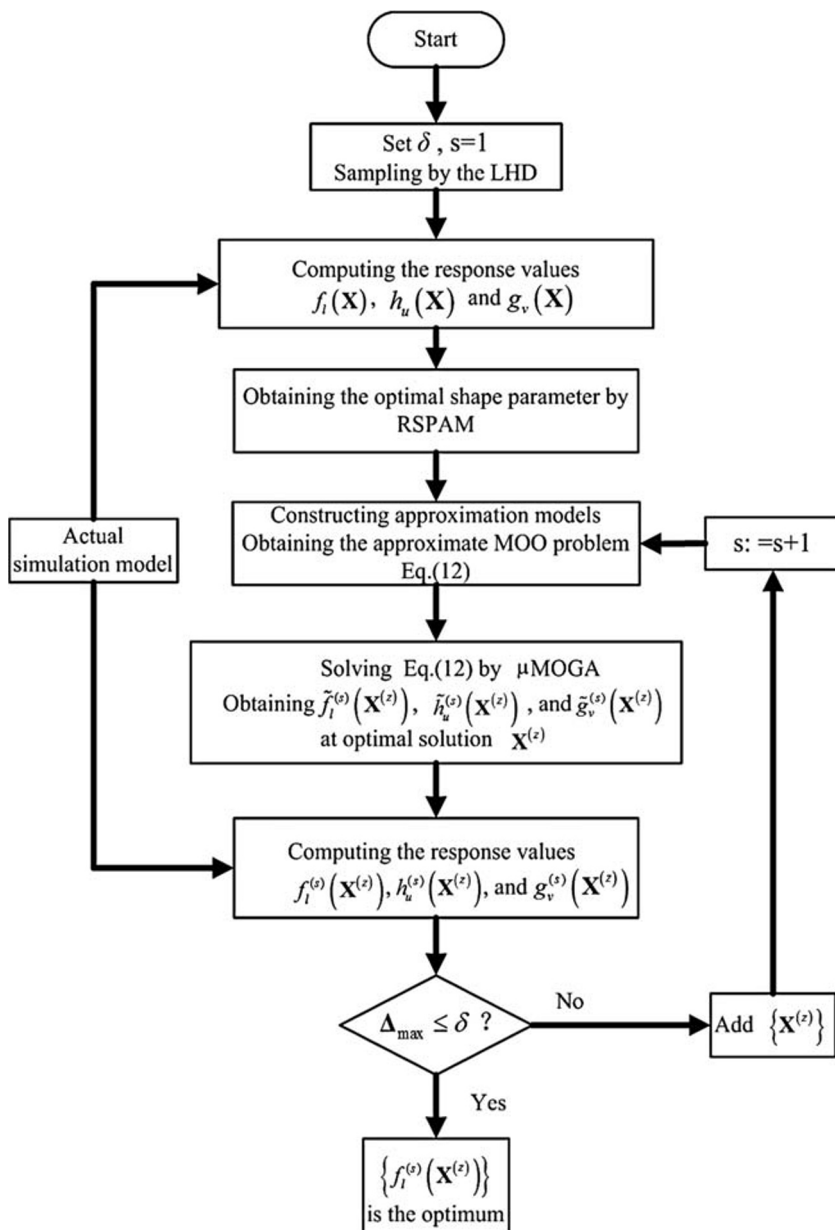
When the coefficient vector \mathbf{w} obtained is substituted into Eq. (2), the approximation model based on RBF is finally constructed. It is noteworthy that the prediction accuracy of the approximation model is significantly affected by the selection of the basic function which is listed in Table 1.

Due to the strong applicability of Gaussian function and its wide application in approximation models, the Gaussian function is chosen for a representative of the basis functions in this paper. The Gaussian function is expressed as follows:

$$h(r_i) = e^{-\varepsilon r_i^2}, r_i = \|\mathbf{X} - \mathbf{X}_i\| \tag{6}$$

where ε denotes the shape parameter. In the process of constructing approximation model, there is usually no obvious formula to describe the intrinsic connections between the shape parameter and the sample points. Moreover, the accuracy of approximation model will be directly affected by the setting of shape parameters. Thus, it is necessary to develop a

Fig. 1 Flowchart of the MOO method based on the adaptive approximation model



more effective method for setting shape parameter to ensure the prediction ability and accuracy of the approximation model.

3.2 Reverse shape parameter analysis method (RSPAM)

According to the construction principle of the above approximation model, the approximation response value at the sample is equal to the actual response value. However, there is a certain error of the approximation model at the predict point. When the initial samples are fixed, the error is related to the selected basis function and its shape parameters. Therefore, a reverse shape parameter analysis method based on the RBF is

developed in this section. Based on this method, the accuracy and efficiency of the approximation models will be greatly enhanced. The following is discussed in detail.

Table 2 The shape parameters under different M values (numerical example A)

M value	Shape parameter (ϵ)			
	$f_1(\mathbf{X})$	$f_2(\mathbf{X})$	$g_1(\mathbf{X})$	$g_2(\mathbf{X})$
M = 4	0.4248	0.3968	0.2363	0.0127
M = 5	0.0984	0.0783	0.2593	0.5904
M = 6	0.0799	0.1552	0.4607	0.3150

Table 3 The count of samples in the iterative process and the corresponding maximum error (numerical example A)

M value	Iterative step	Local-densified samples	Total samples	Maximum error (%)
M = 4	Step 1	0	50	13.74%
	Step 2	2	52	10.25%
	Step 3	1	53	4.65%
M = 5	Step 1	0	50	3.00%
M = 6	Step 1	0	50	7.97%

Firstly, N samples $\Omega_X = \{X_1, \dots, X_j, \dots, X_N\}, j = 1, 2, \dots, N$ containing the key point X_j are given by Latin hypercube design (LHD). Meanwhile, M adjacent sample points $\Omega_{X^k} = \{X_1^k, \dots, X_p^k, \dots, X_M^k\}, p = 1, 2, \dots, M$ and $\Omega_{X^k} \subseteq \Omega_X$, near the key point X_j are used for constructing the mini RBF:

$$\tilde{f}(X) = \sum_{p=1}^M h(r_p) w_p = \sum_{p=1}^M e^{-\varepsilon(\|X-X_p^k\|)^2} w_p \tag{7}$$

In Eq. (7), the coefficient vector $w = (w_1, \dots, w_M)^T$ and the shape parameter ε are two unknown variables which need to be solved. Based on Eq. (5), the coefficient vector $w = (w_1, \dots, w_M)^T$ can be expressed as Eq. (8):

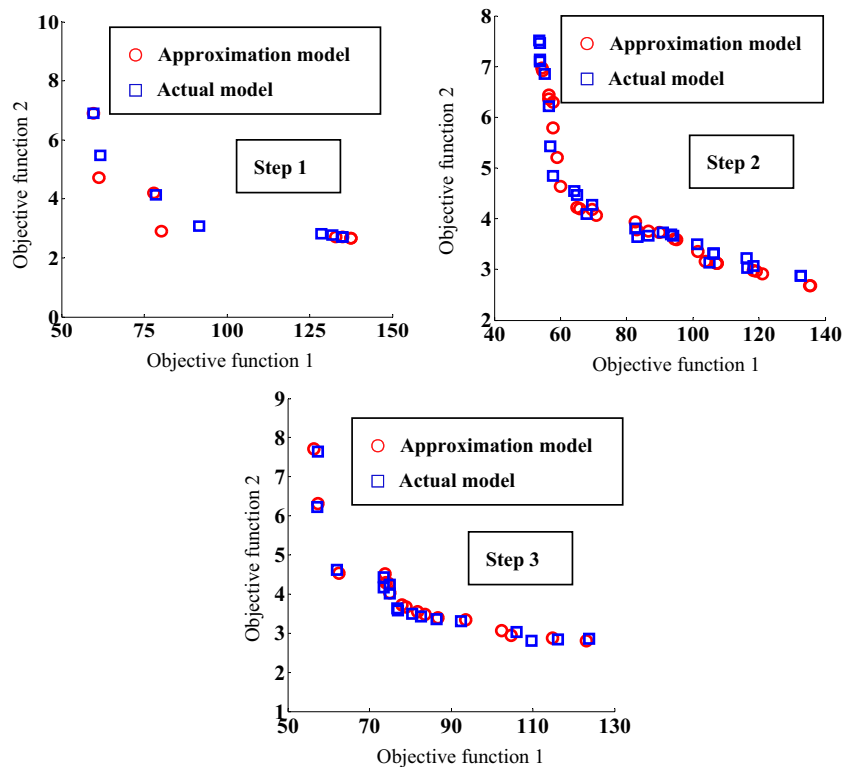
$$w = (w_1, \dots, w_M)^T = \begin{pmatrix} h(\|X_1^k - X_1^k\|) & \dots & h(\|X_1^k - X_M^k\|) \\ \vdots & \ddots & \vdots \\ h(\|X_M^k - X_1^k\|) & \dots & h(\|X_M^k - X_M^k\|) \end{pmatrix}^{-1} \begin{pmatrix} f(X_1^k) \\ \vdots \\ f(X_M^k) \end{pmatrix} \tag{8}$$

Secondly, substituting the key point X_j into the above mini RBF Eq. (7) and assuming that the approximate function value $\tilde{f}(X_j)$ at the key point X_j is equal to the actual value $f(X_j)$, namely:

$$\begin{aligned} f(X_j) &= \tilde{f}(X_j) \\ &= \sum_{p=1}^M h(\|X_j - X_p^k\|) w_p = \sum_{p=1}^M e^{-\varepsilon(\|X_j - X_p^k\|)^2} w_p \\ &= (h(\|X_j - X_1^k\|) \dots h(\|X_j - X_M^k\|)) \cdot (w_1, \dots, w_M)^T \end{aligned} \tag{9}$$

Then, the equation for solving the shape parameter can be obtained by substituting Eq. (8) into Eq. (9) as follows:

Fig. 2 The iterative process and optimization results under $M = 4$ (numerical example A)



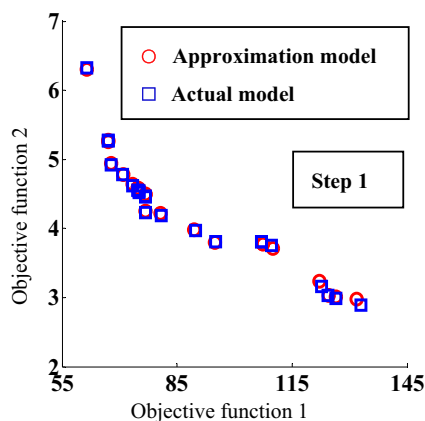


Fig. 3 The iterative process and optimization results under $M = 5$ (numerical example A)

$$\begin{aligned}
 f(\mathbf{X}_j) &= \tilde{f}(\mathbf{X}_j) \\
 &= (h(\|\mathbf{X}_j - \mathbf{X}_1^K\|) \quad \dots \quad h(\|\mathbf{X}_j - \mathbf{X}_M^K\|)) \cdot (w_1, \dots, w_M)^T \\
 &= (h(\|\mathbf{X}_j - \mathbf{X}_1^K\|) \quad \dots \quad h(\|\mathbf{X}_j - \mathbf{X}_M^K\|)) \\
 &\quad \cdot \left(\begin{matrix} h(\|\mathbf{X}_1^K - \mathbf{X}_1^K\|) & \dots & h(\|\mathbf{X}_1^K - \mathbf{X}_M^K\|) \\ \vdots & \ddots & \vdots \\ h(\|\mathbf{X}_M^K - \mathbf{X}_1^K\|) & \dots & h(\|\mathbf{X}_M^K - \mathbf{X}_M^K\|) \end{matrix} \right)^{-1} \begin{pmatrix} f(\mathbf{X}_1^K) \\ \vdots \\ f(\mathbf{X}_M^K) \end{pmatrix}
 \end{aligned} \tag{10}$$

Based on the above analysis, only one unknown variable of shape parameter ε is included, which can be solved by Eq. (10). It is worth noting that a key point and its adjacent samples can be used to obtain a corresponding shape parameter value by solving Eq. (10). Hence, taking N samples $\Omega_{\mathbf{X}} = \{\mathbf{X}_1, \dots, \mathbf{X}_j, \dots, \mathbf{X}_N\}, j = 1, 2, \dots, N$ as key points in turn, N corresponding shape parameters $\Omega_{\varepsilon} = \{\varepsilon_1, \dots, \varepsilon_j, \dots, \varepsilon_N\}, j = 1, 2, \dots, N$ can be obtained by solving the above steps. In this paper, these shape parameters $\Omega_{\varepsilon} = \{\varepsilon_1, \dots, \varepsilon_j, \dots, \varepsilon_N\}$ are called “candidate shape parameters.”

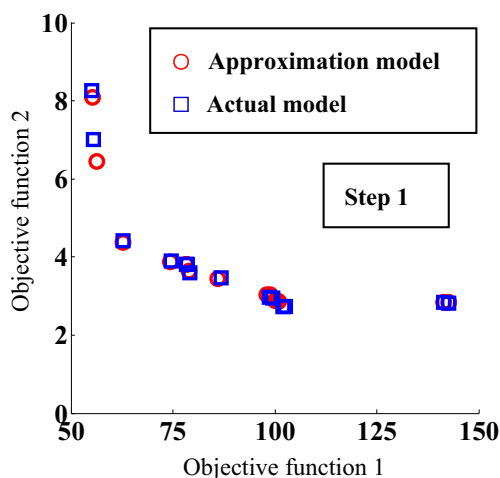


Fig. 4 The iterative process and optimization results under $M = 6$ (numerical example A)

Table 4 The shape parameters based on different methods (numerical example A)

Method	Shape parameter (ε)			
	$f_1(\mathbf{X})$	$f_2(\mathbf{X})$	$g_1(\mathbf{X})$	$g_2(\mathbf{X})$
RSPAM ($M = 5$)	0.0984	0.0783	0.2593	0.5904
Long’s method	1.0460	1.0460	1.0460	1.0460
Koupaei’s method	0.0010	0.1230	0.0010	0.0010

Thirdly, N candidate shape parameters $\Omega_{\varepsilon} = \{\varepsilon_1, \dots, \varepsilon_j, \dots, \varepsilon_N\}$ are used to construct N test approximation models, respectively, and the error analysis is also performed for every test approximation model. The candidate shape parameter with the minimum error is identified as the optimal shape parameter for constructing the approximation model. The detailed process is as follows:

The samples $\Omega_{\mathbf{X}} = \{\mathbf{X}_1, \dots, \mathbf{X}_j, \dots, \mathbf{X}_N\}$ are divided into two parts according to the sample number. The first half of the samples $\{\mathbf{X}_1, \dots, \mathbf{X}_{N/2}\}$ are used as the “the construction points,” and the second half of the samples $\{\mathbf{X}_{N/2+1}, \dots, \mathbf{X}_N\}$ are chosen as the “the test points.” The construction points are combined with each candidate shape parameter ε_j to construct corresponding approximation model, and the test points are adopted to evaluate the prediction ability of the approximation model through the error criterion σ_j defined by Eq. (11).

$$\begin{aligned}
 \sigma_j &= \frac{\sum_{t=\frac{N}{2}+1}^N \left| \frac{f(\mathbf{X}_t) - \tilde{f}(\mathbf{X}_t)}{f(\mathbf{X}_t)} \right|}{\frac{N}{2}}, \quad j = 1, 2, \dots, N, t \\
 &= \frac{N}{2} + 1, \dots, N
 \end{aligned} \tag{11}$$

where $f(\mathbf{X}_t)$ denotes the actual value at the test point and $\tilde{f}(\mathbf{X}_t)$ represents the approximate value of the function at the test point. After all the errors corresponding to candidate shape parameters are obtained, the shape parameter with the minimum error is chosen for the optimal shape parameter.

Finally, the samples $\Omega_{\mathbf{X}} = \{\mathbf{X}_1, \dots, \mathbf{X}_N\}$ are combined with the optimal shape parameter to construct the final approximation model.

3.3 Local-densifying approximation method

When the approximation models of objective functions and its corresponding constraints are constructed based on the RBF, the MOO problem in Eq. (1) becomes the following approximate MOO problem:

Table 5 The count of samples in the iterative process and the corresponding maximum error (numerical example A)

Method	Iterative step	Local-densified samples	Total samples	Maximum error (%)
RSPAM (M = 5)	Step 1	0	50	3.00%
Koupaei's method	Step 1	0	50	6.46%
Long's method	Step 1	0	50	28.90%
	Step 2	4	54	19.04%
	Step 3	2	56	30.58%
	Step 4	3	59	8.80%

$$\begin{aligned}
 \min_{\mathbf{X}} \quad & \tilde{f}_l(\mathbf{X}), l = 1, 2, \dots, a \text{ s.t. } \tilde{h}_u(\mathbf{X}) = 0, u \\
 & = 1, \dots, b \tilde{g}_v(\mathbf{X}) \leq 0, v = 1, \dots, c \mathbf{X} \\
 & = (X_1, X_d, \dots, X_n)^T, d = 1, \dots, n
 \end{aligned} \tag{12}$$

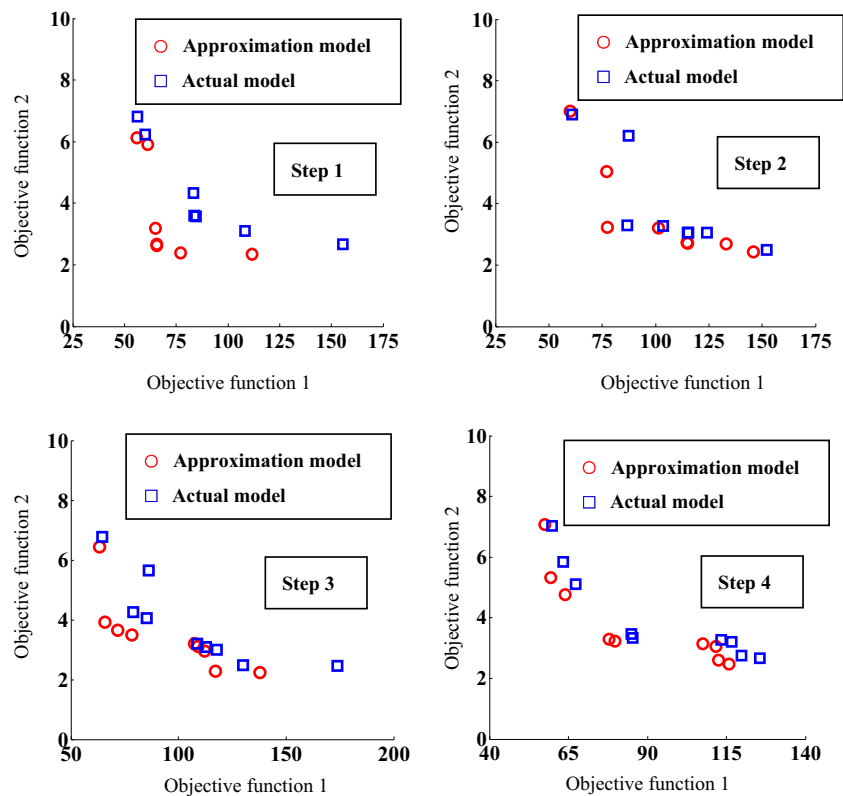
where $\tilde{f}_l(\mathbf{X})$, $\tilde{h}_u(\mathbf{X})$, and $\tilde{g}_v(\mathbf{X})$ represent approximation models of the objective function, the equality constraint, and the inequality constraint, which are explicit functions with respect to the design vector \mathbf{X} .

For the approximation MOO problem in Eq. (12), the Pareto optimal set of objective functions and their corresponding constraint function values are primarily concerned. Considering the accuracy of the abovementioned approximate models depend largely on the samples in the experimental design space, hence, it is necessary to arrange the samples more reasonably so that the limited samples are more

distributed near the region where the Pareto optimal set are found. When the prediction ability and accuracy of the approximation model are ensured in the local area where the Pareto optimal set are found, more reliable optimization results can be obtained.

For these reasons, the local-densifying approximation method is applied to enhance the local precision of approximation models in the Pareto optimal set, which is the main mechanism of the adaptive approximation model. The local-densifying approximation method is an updating strategy of sampling method which concentrates limited sample resources to the local regions we concerned, namely, more samples are expected to be densified into the local regions where the Pareto optimal set are found. In the local-densifying approximation method, the Pareto optimal set are obtained and evaluated in each iteration step. According to the approximation values at the optimal Pareto set, the approximation

Fig. 5 The iterative process and optimization results based on the Long's method (numerical example A)



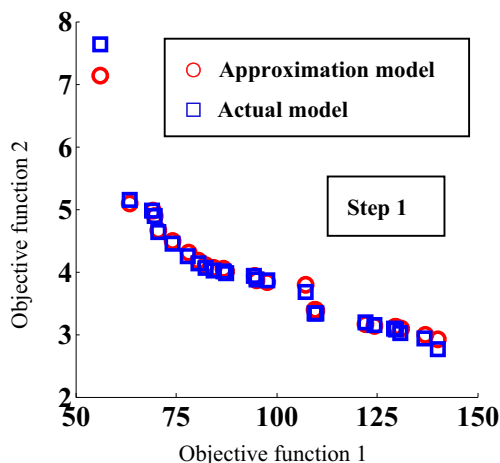


Fig. 6 The iterative process and optimization results based on the Koupaei’s method (numerical example A)

models are updated by adding local-densified samples to the sample space for next iteration until the stop criteria are satisfied. Therefore, it ensures that the approximation models have small approximate errors in the Pareto optimal set and the result can be more reliable.

3.4 Computational procedure

In this method, the micro multi-objective genetic algorithm (μ MOGA) (Liu et al. 2012) is applied to solve the MOO problem in Eq. (12) due to the μ MOGA has an outstanding performance in searching the Pareto optimal set. The computational procedure of the proposed MOO method is given in Fig. 1 and the details are outlined as:

- (1) Sampling in the design vector space by the LHD. Set the allowable error δ and initial iteration step $s = 1$.
- (2) According to the above initial samples, computing the actual response values of the objective function $f_i(\mathbf{X})$ and constraints $h_u(\mathbf{X})$ and $g_v(\mathbf{X})$ evaluated by the actual simulation model.
- (3) Obtaining the optimal shape parameter by using Reverse shape parameter analysis method.
- (4) Constructing approximation models of the objective function and constraints and obtaining the approximate MOO problem as Eq. (12).

Fig. 7 The structure of I-beam

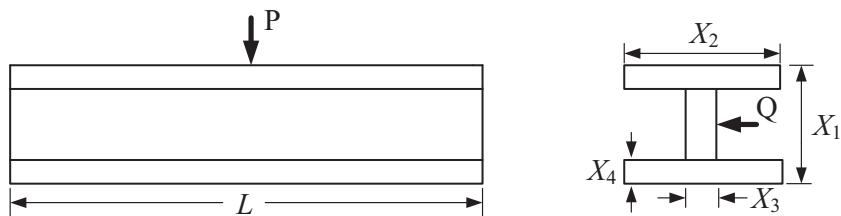


Table 6 The shape parameters under different M values (numerical example B)

M value	Shape parameter (ϵ)		
	$f_1(\mathbf{X})$	$f_2(\mathbf{X})$	$g(\mathbf{X})$
M = 4	0.6657	0.3412	0.1448
M = 5	0.3874	0.1196	0.2969
M = 6	0.4258	0.3817	0.4296

- (5) Solving the approximate MOO problem Eq. (12) by μ MOGA and obtaining the Pareto optimal set of the approximation objective function $\{\tilde{f}_i^{(s)}(\mathbf{X}^{(z)})\}$, $z = 1, 2, \dots, t$, where $\tilde{f}_i^{(s)}(\mathbf{X}^{(z)})$ stands for the z th Pareto solution of the Pareto optimal set in step s ; Similarly, their corresponding approximation constraint function values $\tilde{h}_u^{(s)}(\mathbf{X}^{(z)})$ and $\tilde{g}_v^{(s)}(\mathbf{X}^{(z)})$ at optimal solution $\mathbf{X}^{(z)}$ also can be obtained.
- (6) Based on the simulation model, computing the actual response values of the objective function $\{f_i^{(s)}(\mathbf{X}^{(z)})\}$, $z = 1, 2, \dots, t$, and their corresponding actual constraint function values $h_u^{(s)}(\mathbf{X}^{(z)})$ and $g_v^{(s)}(\mathbf{X}^{(z)})$.
- (7) Calculating the maximum error Δ_{\max} :

$$\Delta_{\max} = \max\{\Delta_z\}, \quad z = 1, 2, \dots, t$$

$$\Delta_z = \max\left\{\left|\frac{f_i^{(s)}(\mathbf{X}^{(z)}) - \tilde{f}_i^{(s)}(\mathbf{X}^{(z)})}{f_i^{(s)}(\mathbf{X}^{(z)})}\right|, \left|\frac{h_u^{(s)}(\mathbf{X}^{(z)}) - \tilde{h}_u^{(s)}(\mathbf{X}^{(z)})}{h_u^{(s)}(\mathbf{X}^{(z)})}\right|, \left|\frac{g_v^{(s)}(\mathbf{X}^{(z)}) - \tilde{g}_v^{(s)}(\mathbf{X}^{(z)})}{g_v^{(s)}(\mathbf{X}^{(z)})}\right|\right\}$$

If $\Delta_{\max} \leq \delta$, then $\{f_i^{(s)}(\mathbf{X}^{(z)})\}$ and $z = 1, 2, \dots, t$ are determined as the final solution and the iteration terminates. Otherwise, updating the approximation models by adding the optimal set $\{\mathbf{X}^{(z)}\}$ with error more than δ to the sample space. Set $s = s + 1$ and move to step (4).

4 Numerical examples and discussion

In this section, the accuracy of optimization results and the efficiency of the algorithm are tested by two numerical examples. Meanwhile, the proposed method is also performed to

Table 7 The count of samples in the iterative process and the corresponding maximum error (numerical example B)

M value	Iterative step	Local-densified samples	Total samples	Maximum error (%)
M = 4	Step 1	0	50	38.30%
	Step 2	3	53	16.96%
	Step 3	5	58	6.60%
M = 5	Step 1	0	50	11.96%
	Step 2	1	51	7.22%
M = 6	Step 1	0	50	18.15%
	Step 2	4	54	13.29%
	Step 3	2	56	7.24%

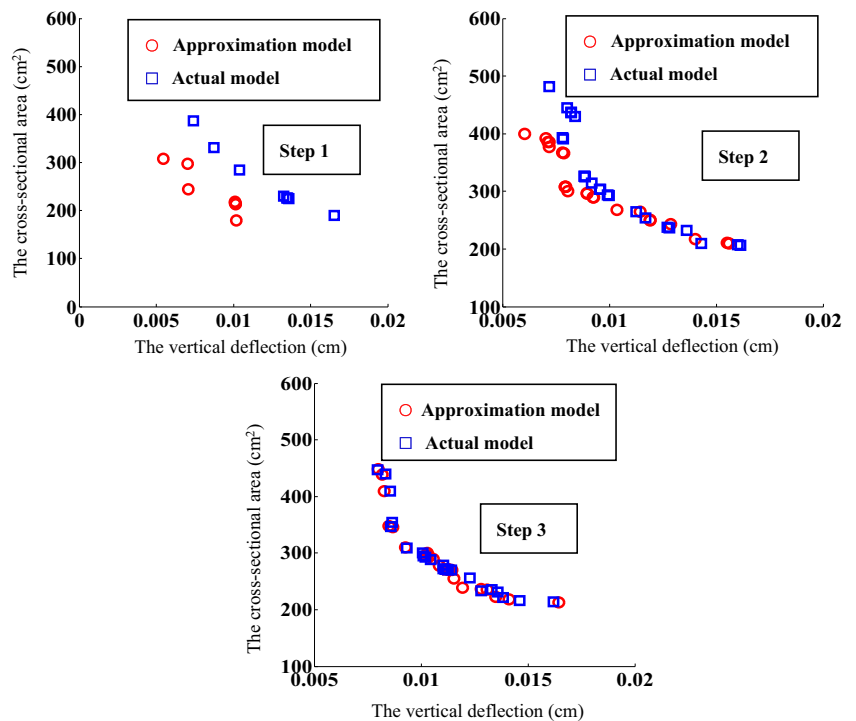
demonstrate its practical engineering applicability through two actual engineering examples.

4.1 Numerical example A

In the numerical example A, a two-objective optimization problem with two constraints is as follows:

$$\begin{aligned}
 \min_{\mathbf{X}} f_1(\mathbf{X}) &= -X_1X_2 + X_3X_4/2 \\
 f_2(\mathbf{X}) &= 2X_1X_2/X_4^2 + 3X_2X_4/X_3^2 \\
 s.t. \quad g_1(\mathbf{X}) &= 10 - 2X_1 - X_2/X_3 + X_4 \leq 0 \\
 g_2(\mathbf{X}) &= 65 - X_2 + X_1/X_4 - 5X_3 \leq 0 \\
 \mathbf{X} &= (X_1, X_2, X_3, X_4)^T, 10 \leq X_1, X_2, X_3, X_4 \leq 20
 \end{aligned} \tag{13}$$

Fig. 8 The iterative process and optimization results under M = 4 (numerical example B)

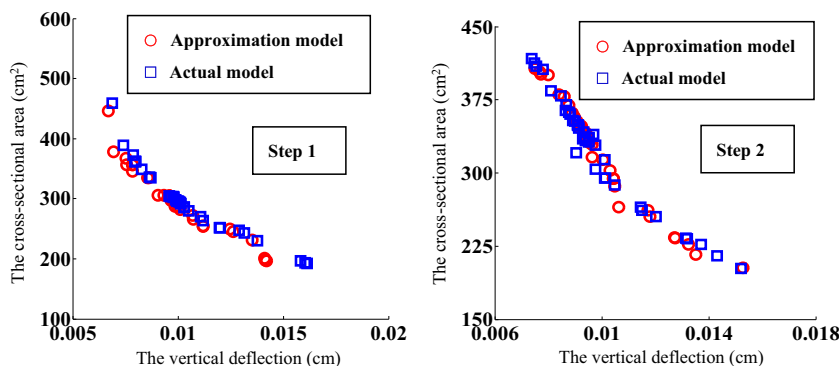


where $f_1(\mathbf{X})$ and $f_2(\mathbf{X})$ represent the objective function 1 and the objective function 2, respectively. $g_1(\mathbf{X})$ and $g_2(\mathbf{X})$ are the inequality constraints. The \mathbf{X} stands for the design vector. The allowable error δ is set to 0.1. The μ MOGA and local-densifying approximation method are also applied to solve the Pareto optimal set. The preset parameters for the μ MOGA are as follows: the maximum generation is 200, the population size is 5.0, and the probability of crossover is 0.5. To analyze the influence of the shape parameters for the optimization results, the abovementioned problem is investigated for two cases.

4.1.1 The influence of the number of adjacent sample points

In this case, the influence of the number of adjacent sample points M on the optimization results is discussed. Meanwhile, the local-densifying approximation method is adopted to improve the accuracy of Pareto optimal set. The fifty initial

Fig. 9 The iterative process and optimization results under $M = 5$ (numerical example B)



samples are generated by the LHD and the number of adjacent sample points M is varied between 4 and 6 in steps of 1. The proposed RSPAM is used to solve the shape parameters of the RBFs, and the corresponding approximation models of the objective functions and constraints are constructed based on the initial samples and these shape parameters. The obtained shape parameters of the approximation models under different M values are listed in Table 2, and the iterative process with optimization results are presented in Figs. 2, 3, and 4. Simultaneously, the numbers of samples in the iterative process and the corresponding maximum error are detailed in Table 3.

According to Fig. 2, when $M = 4$, the maximum error of the functions at the Pareto optimal set is 13.74% in step 1. The iterative process indicates that the prediction ability of the

approximation model is improved through adding local-densified samples to the sample space, and in step 3, the corresponding maximal error of the objective functions and constraint functions is found to be 4.65%. The result implies that the Pareto optimal set satisfying the allowable error are obtained by three iterative steps. While the number of adjacent sample points M is set to $M = 5$ and $M = 6$, the final Pareto optimal set satisfying the allowable error are obtained by one iterative step which are presented in Figs. 3 and 4. The corresponding maximum errors are 3.0% and 7.97%, respectively. According to the above computational results, when $M = 4$, more iterative steps are needed to obtain the final Pareto optimal set because the insufficient sample information is available to solve shape parameters. Meanwhile, the maximum error of $M = 6$ is more than that of $M = 5$ because the ill-

Fig. 10 The iterative process and optimization results under $M = 6$ (numerical example B)

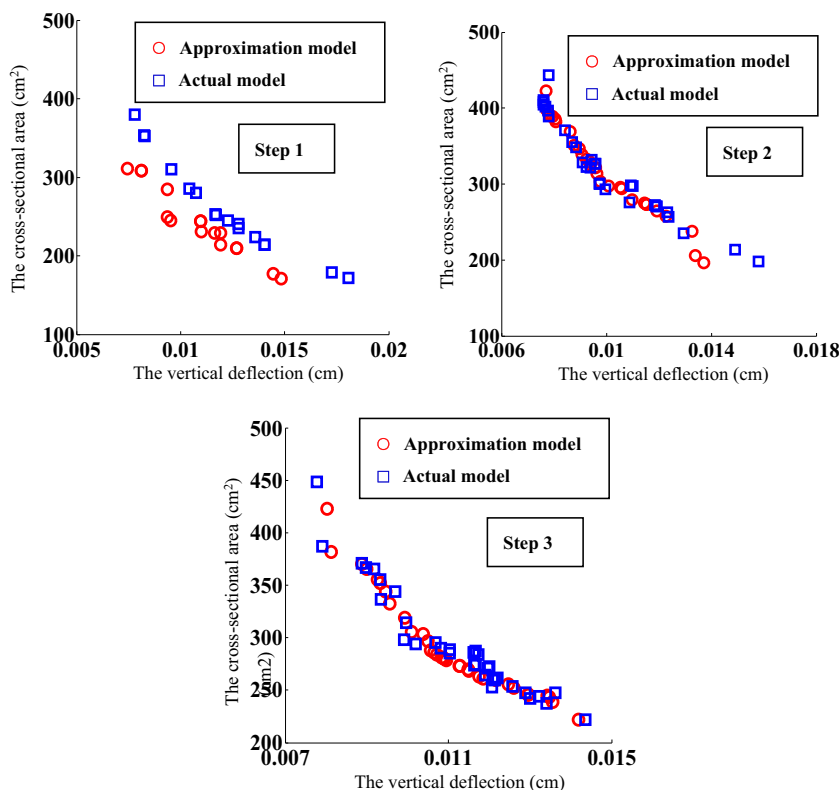


Table 8 The shape parameters based on different methods (numerical example B)

Method	Shape parameter (ε)		
	$f_1(\mathbf{X})$	$f_2(\mathbf{X})$	$g(\mathbf{X})$
RSPAM (M = 5)	0.3874	0.1196	0.2969
Long's method	0.8132	0.8132	0.8132
Koupaei's method	0.3520	0.0010	0.3100

conditioned matrix appears many times in the solving process of shape parameters. It is obvious that the selection of the number of adjacent sample points M will directly affect the ability of the algorithm to obtain the expected optimization results. According to the above optimization results, when the number of adjacent sample points M is varied between 4 and 6, five adjacent sample points ($M = 5$) will be helpful to improve the accuracy of optimization results and the efficiency of the algorithm in this representative case.

4.1.2 The computational efficiency and optimization accuracy

This case is the verification of the proposed MOO method in the computational efficiency and optimization accuracy. The RSPAM is compared with Long's method (Long et al. 2016) and Koupaei's method (Koupaei et al. 2018) for calculating the shape parameters of the RBFs. In the proposed RSPAM, five adjacent sample points ($M = 5$) could be recommended to solve the optimal shape parameter according to the above optimization results. In the Long's method, the formula of solving shape parameters ε_L is expressed as:

$$\varepsilon_L = ((\max(\mathbf{X}) - \min(\mathbf{X})) / N)^{\frac{1}{n}} \tag{14}$$

where $(\max(\mathbf{X}) - \min(\mathbf{X}))$ represents the longest distance in the sample points. N and n stand for the number of sample points and the dimension of design variables, respectively.

Table 9 The count of samples in the iterative process and the corresponding maximum error (numerical example B)

Method	Iterative step	Local-densified samples	Total samples	Maximum error (%)
RSPAM (M = 5)	Step 1	0	50	11.96%
	Step 2	1	51	7.22%
Koupaei's method	Step 1	0	50	25.86%
	Step 2	2	52	10.43%
	Step 3	2	54	6.59%
Long's method	Step 1	0	50	66.49%
	Step 2	2	52	77.26%
	Step 3	2	54	46.50%
	Step 4	2	56	55.53%
	Step 5	1	57	22.26%

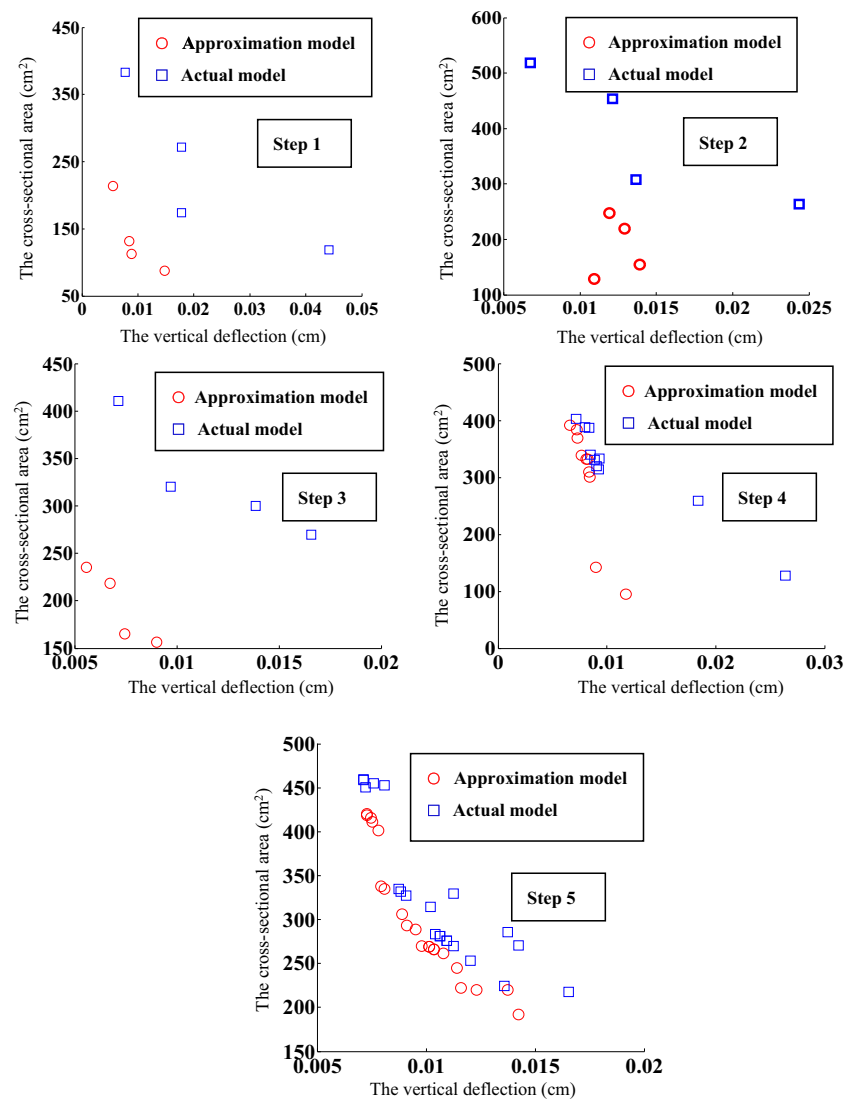
In Koupaei's method, the shape parameter ε_k can be solved by the following optimization problem:

$$\min_{\varepsilon_k} RMS(\varepsilon_k) = \sqrt{\frac{1}{\varpi} \sum_{i=1}^{\varpi} |f(\mathbf{X}_i) - \tilde{f}(\mathbf{X}_i, \varepsilon_k)|^2} \tag{15}$$

where $RMS(\varepsilon_k)$ represents the root mean square (RMS) error with respect to the shape parameter ε_k . $f(\mathbf{X}_i)$ and $\tilde{f}(\mathbf{X}_i, \varepsilon_k)$ denote the actual function and approximate function, respectively. $\mathbf{X}_i, i = 1, \dots, \varpi$ is the test point, and ϖ stands for the number of the test points. The number of initial samples is 50, and the proposed RSPAM ($M = 5$), Long's method, and Koupaei's method are used to solve the shape parameters of the RBFs as listed in Table 4, respectively. Then, the corresponding approximation models of the objective functions and constraint are constructed based on these samples and shape parameters.

The iterative process and optimization results under the methods of Long and Koupaei are shown in Figs. 5 and 6. The count of samples in the iterative process and the corresponding maximum error are detailed in Table 5. It is obvious that the proposed method and Koupaei's method can obtain the Pareto optimal set satisfying the allowable error in step 1. The corresponding maximum errors of the Pareto optimal set are 3.0% and 6.46%, respectively. However, the errors of the Pareto optimal set in step 1 are not less than allowable error 10% by using the Long's method. The corresponding maximal error of the objective functions and constraint functions is found to be 28.90%, which suggests the approximation models are relatively coarse by using the methods of the Long's method. Through adding local-densified samples to the sample space in the iterative process, the maximum error is 8.80% in step 4 for the Long's method, which demonstrates the optimization results have reached the allowable error requirement after 4 steps. The optimization results show that the Pareto optimal set obtained by the proposed MOO method in step 1 are obviously better than that obtained by the methods of Koupaei and Long. The results also indicate that the

Fig. 11 The iterative process and optimization results based on the Long's method (numerical example B)



optimal shape parameters obtained by the RSPAM could ensure the accuracy of the approximation model at the initial step.

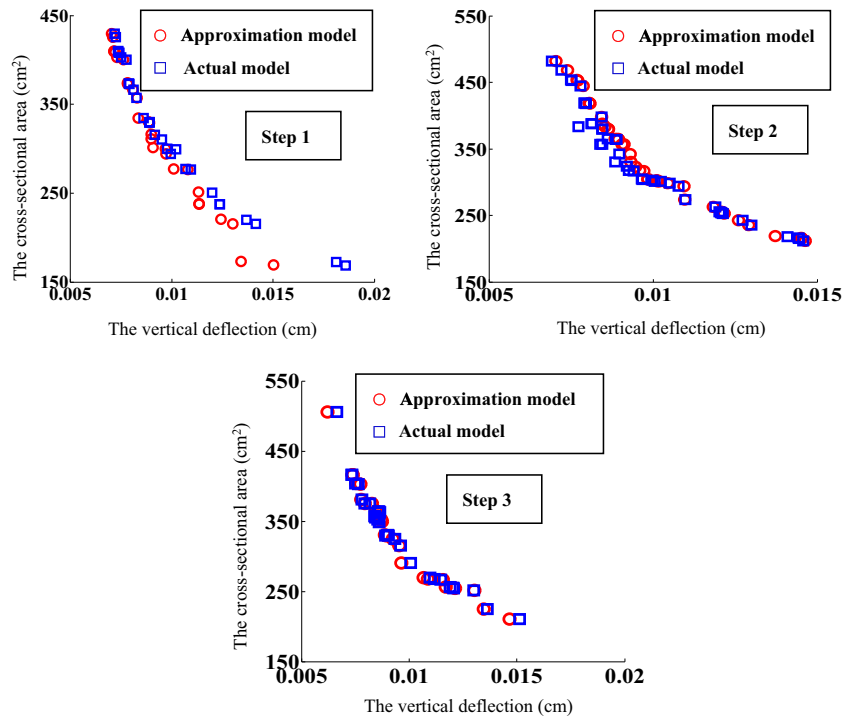
From the calculation results of three different methods, the proposed method could obtain the optimal solutions more efficiently. This is because the Koupaei's method mainly focuses on the minimum RMS and ignores the internal relationship of the initial sample points. Simultaneously, the Long's method only solve the shape parameters through the number of sample points and design variables, which uses the same shape parameters to construct approximation models, namely, the characteristics of the nonlinear objective functions and constraints are not considered in the Long's method. However, the proposed method solves the corresponding shape parameters for different nonlinear objective functions and constraints based on the internal relation of the initial sample points, namely, the different shape

parameters are used to construct the approximation models of the nonlinear objective functions and constraints than only the number of sample points and design variables are considered.

4.2 Numerical example B

An optimization design problem of I-beam is illustrated in Fig. 7. The length L of the I-beam is 200 cm. Two loads are applied to the I-beam as shown in the Fig. 7, which are $P = 600\text{ kN}$ and $Q = 50\text{ kN}$, respectively. The Young's modulus of the I-beam is $E = 200\text{ GPa}$. The above MOO problem can be defined as minimizing the cross-sectional area and vertical deflection of the I-beam under the constraint of principal stress below the allowable stress $\sigma = 6\text{ kN/cm}^2$. The parameters of the I-beam are considered as the design variables which are X_1, X_2, X_3 , and X_4 . Therefore, the above MOO problem is formulated as:

Fig. 12 The iterative process and optimization results based on the Koupaei’s method (numerical example B)



$$\begin{aligned} & \min_{\mathbf{X}} (f_1(\mathbf{X}), f_2(\mathbf{X})) \\ & f_1(\mathbf{X}) = 2X_2X_4 + X_3(X_1 - 2X_4) \\ & f_2(\mathbf{X}) = \frac{PL^3}{48EI} = \frac{5000}{\frac{1}{12}X_3(X_1 - 2X_4)^3 + \frac{1}{6}X_2X_4^3 + 2X_2X_4\left(\frac{X_1 - X_4}{2}\right)^2} \\ & s.t. g(\mathbf{X}) = \frac{180000X_1}{X_3(X_1 - 2X_4)^3 + 2X_2X_4[4X_4^2 + 3X_1(X_1 - 2X_4)]} + \frac{15000X_2}{(X_1 - 2X_4)X_3^3 + 2X_4X_2^3} \leq 6 \\ & \mathbf{X} = (X_1, X_2, X_3, X_4)^T \quad 70\text{cm} \leq X_1 \leq 90\text{cm}, 40\text{cm} \leq X_2 \leq 60\text{cm}, 0.5\text{cm} \\ & \quad \leq X_3 \leq 2\text{cm}, 1\text{cm} \leq X_4 \leq 3\text{cm} \end{aligned} \tag{16}$$

where $f_1(\mathbf{X})$ and $f_2(\mathbf{X})$ represent the cross-sectional area and vertical deflection of the I-beam, respectively. $g(\mathbf{X})$ is the principal stress. In the optimization process, the allowable error δ is set to 0.1. The Pareto optimal set is found by using the μ MOGA and local-densifying approximation method. The parameters for μ MOGA are preset as follows: the

maximum generation is 200, the population size is 5.0, and the probability of crossover is 0.5, respectively. To discuss the influence of the shape parameters for the optimization results, the abovementioned MOO problem is investigated for two cases.

4.2.1 The influence of the number of adjacent sample points

In this case, the shape parameters of the RBFs are solved by the proposed RSPAM and the accuracy of Pareto optimal set is ensured by using the local-densifying approximation method. The number of adjacent sample points M is set to 4, 5, and 6, respectively. The shape parameters under different M values are presented in Table 6 and the iterative process with optimization results are displayed in Figs. 8, 9, and 10. For better illustration of the influence on the optimization results under different number of adjacent sample points M , the count of samples in the iterative process and the maximum error in each step are detailed in Table 7.

In step 1, the approximation models are constructed by using 50 initial samples which are generated by the LHD. The corresponding maximal error of the objective functions and constraint functions are found to be 38.30%, 11.96%, and 18.15% under three different number of adjacent sample points, respectively. The results indicate that the local-densifying approximation method has to be employed for strengthening the accuracy of approximation models. In step 2, The Pareto optimal set with 5 adjacent sample points has reached the allowable error requirement and the maximal error of the objective functions and constraints is found to be

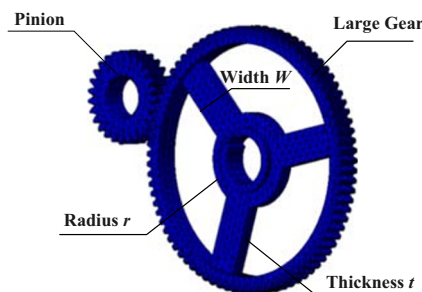


Fig. 13 The structure of gear

Table 10 The count of samples in the iterative process and the corresponding maximum error (engineering example A)

Iterative step	Local-densified samples	Total samples	Maximum error (%)
Step 1	0	30	75.25%
Step 2	4	34	47.54%
Step 3	4	38	8.61%

7.22%. However, the Pareto optimal set of the other two adjacent sample points still fails to meet the allowable error requirement. Through adding local-densified samples to the sample space, both $M = 4$ and $M = 6$ reach the allowable error requirements in step 3. The corresponding maximum error is 6.60% and 7.24%, respectively.

According to the above results, the accuracy and efficiency of the optimization are greatly influenced by the number of adjacent sample points M . Generally, the accuracy of optimization results will be relatively low when the fewer adjacent sample points are used to solve Eq. (10). When more adjacent sample points are selected, the accuracy of optimization results may be improved but ill-conditioned matrices may appear in the process of solving Eq. (10) which will lead to the failure of solution and low efficiency. In the above cases, $M = 4$ to 6 are investigated and the optimization results demonstrate that the accuracy and efficiency of the proposed method can be well satisfied when $M = 5$. It is noteworthy that the number of adjacent sample points M could also be determined by a trade-off between the accuracy and efficiency from the operator. Meanwhile, more cases of different M values have been included in the future work.

4.2.2 The computational efficiency and optimization accuracy

The reverse shape parameter analysis method (RSPAM, $M = 5$), Long's method, and Koupaei's method are used again to solve the shape parameters of the RBFs, respectively. The

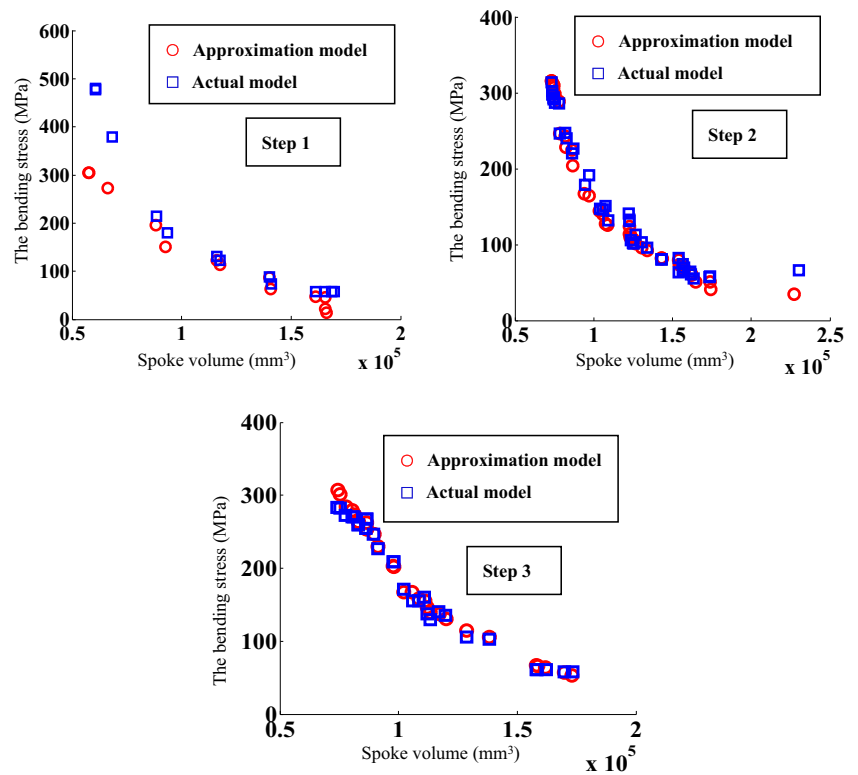
Table 11 The Pareto solutions satisfying the requirement (engineering example A)

No.	t	W	r	$P(\text{MPa})$	$V(\text{mm}^3)$
1	5.267	31.031	40.571	283.457	74,220.779
2	5.267	31.956	42.741	272.891	77,730.862
3	5.618	31.485	41.961	270.593	81,274.061
4	5.618	31.954	42.742	259.994	82,916.882
5	6.204	31.074	42.742	246.701	89,541.361
6	6.077	33.235	41.229	227.000	91,261.305
7	6.193	34.824	42.351	208.663	97,653.196
8	5.896	45.606	42.977	140.869	117,003.927
9	5.490	71.861	40.547	61.060	162,229.604
10	5.352	77.733	41.251	58.053	169,960.726

shape parameters obtained by the different methods are listed in Table 8. Based on these shape parameters and the initial samples, the corresponding approximation models of the objective functions and constraints are constructed. The other preset parameters keep unchanged. The iterative process and optimization results under the methods of Long and Koupaei are presented in Figs. 11 and 12. Meanwhile, the count of samples in the iterative process and the corresponding maximum error are detailed in Table 9.

Based on the above optimization results, the maximal error of the objective functions and constraint functions based on the proposed method is 11.96% in step 1, which is very close to the allowable error value. It indicates that the optimal shape parameters obtained by the RSPAM could ensure the accuracy of the approximation model at the beginning of iteration. With the increasing of sample points by employing local-densifying approximation method, the Pareto optimal set satisfying the allowable error are obtained by the proposed MOO method in step 2 and the corresponding maximal error of the objective functions and constraint functions is found to be 7.22%, which is obviously better than other methods. While the errors of the other methods are not less than the allowable error 10% in step 2, which shows that the methods of Long and Koupaei need more iterative steps to obtain the Pareto optimal set for meeting the accuracy requirements. By using the local-densifying approximation method, the maximal error of the objective functions and constraint functions for the Koupaei's method is 6.59% in step 3, which indicates the optimization results have reached the allowable error requirement after 3 steps. However, the corresponding maximal error based on the Long's method is 22.26% in step 5, which demonstrates the Pareto optimal set still fail to meet the allowable error requirement. This is because the Long's method only consider the influence of the number of sample points and design variables, so that the shape parameters of three approximation models $\tilde{f}_1(\mathbf{X})$, $\tilde{f}_2(\mathbf{X})$, and $\tilde{g}(\mathbf{X})$ are the same. It induces the accuracy of the approximation models needs to be improved by more iterative steps, while the RSPAM fully considers the influence of different objective functions and constraints based on the internal relation of the initial sample points, and the corresponding approximation models are constructed by using the different shape parameters. Therefore, the proposed

Fig. 14 The iterative process and optimization results (engineering example A)



method could get more accurate approximation model and solve the optimal solutions more quickly than other two methods.

4.3 Engineering example A

Gear transmission is one of the most common drive forms of mechanical transmission system. The gear transmission structure will directly affect the transmission efficiency of mechanical system. Hence, the proposed method is used to design a practical gear transmission structure. As shown in Fig. 13, the numerical model of the gear transmission structure is constructed, which consists of main gear and pinion. Minimizing the spokes volume and the bending stress of the

main gear are two objectives for this design problem. During the transmission process, the spoke thickness t , spoke width W , and spoke radius r will play important roles in the bending stress of the main gear. Thus, the spoke thickness t , spoke width W , and spoke radius r are considered as the design variables. The other parameters in the gear system are as follows: the modulus of the gear is $m = 4$, the diameter of pinion is 108 mm, the diameter of gear is 324 mm, the material of the gear is 45# steel, the permissible bending stress is 325.08 MPa, the torque of pinion gear is $T = 286500 \text{ N} \cdot \text{mm}$, and the periphery force of the tooth surface is $F_t = 5305.5 \text{ N}$. The optimization problem can be described as follows:

$$\min_{t, W, r} (P(t, W, r), V(t, W, r)) \quad 5\text{mm} \leq t \leq 10\text{mm}, 20\text{mm} \leq W \leq 80\text{mm}, 40\text{mm} \leq r \leq 65\text{mm} \quad (17)$$

where $P(t, W, r)$ stands for the bending stress of the main gear and $V(t, W, r)$ is the spoke volume.

In the optimization process, the allowable error δ is set to 0.1. The μ MOGA and local-densifying approximation method are also used to solve the Pareto optimal set. The preset parameters for μ MOGA are as follows: the maximum generation is 200, and the population size and the probability of crossover are 5.0 and 0.5. The approximation models of functions $P(t, W, r)$ and $V(t, W, r)$ are constructed by using 30 initial samples which are generated by the LHD. Based on the

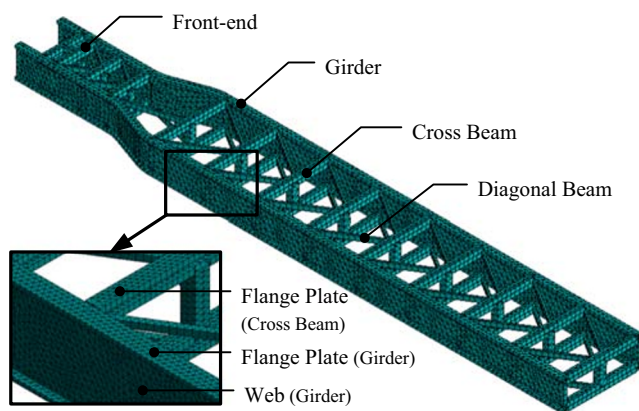


Fig. 15 The forearm structure of the bucket wheel stacker-reclaimer

Table 12 The count of samples in the iterative process and the corresponding maximum error (engineering example B)

Iterative step	Local-densified samples	Total samples	Maximum error (%)
Step 1	0	30	7.35%
Step 2	2	32	1.08%

proposed RSPAM ($M = 5$), the optimal shape parameters are solved for the approximation models, which are 0.5344 and 0.1827 for the approximation models $\tilde{P}(t, W, r)$ and $\tilde{V}(t, W, r)$, respectively. Under the help of the proposed method, the iterative process is displayed in Fig. 14 and the count of samples in the iterative steps are detailed in Table 10. It can be found in step 1, the Pareto optimal set of approximate functions $\tilde{P}(t, W, r)$ and $\tilde{V}(t, W, r)$ are far from the actual function $P(t, W, r)$ and $V(t, W, r)$, which obviously shows that the approximation models are not accurate enough. Through the local-densifying approximation method for three iterative steps, the maximal error of the objective functions has been reduced to 8.61%, which indicates the Pareto optimal sets have satisfied the allowable error. Hence, ten solutions are chosen from the Pareto solutions given in Table 11. The engineers will select the No.10 solution if the bending stress of the main gear is the primary concern. Alternatively, if more attention to the spoke volume is paid, the No.1 solution would be considered.

4.4 Engineering example B

The forearm structure is one of the most important parts of the bucket wheel stacker-reclaimer. When the bucket wheel stacker-reclaimer is in operation, the 9600-kg bucket wheel is installed at the front end of the forearm structure. To enhance the safety performance of forearm structure, and reduce the weight to satisfy the requirements of lightweight design,

Table 13 The Pareto solutions satisfying the requirement (engineering example B)

No.	X_1	X_2	X_3	X_4	$P(\text{MPa})$	$M(\text{kg})$
1	10.286	12.476	13.714	13.810	154.65	16,185
2	8.476	9.810	8.095	11.905	178.97	12,760
3	10.286	9.429	8.857	14.000	156.50	14,532
4	8.381	10.000	8.667	12.286	175.04	12,989
5	8.286	11.143	8.000	13.333	166.48	13,116
6	11.429	10.095	9.333	13.714	156.02	15,318
7	9.048	8.286	10.571	13.714	160.24	14,139
8	11.048	8.476	13.524	13.619	154.95	16,147
9	8.762	9.619	8.667	13.333	164.98	13,444
10	8.571	11.810	8.571	13.714	162.35	13,608
11	9.714	10.190	8.286	13.333	163.09	13,935

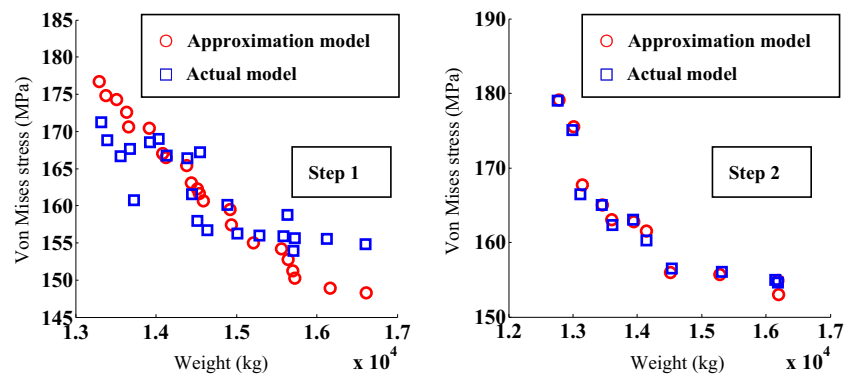
the proposed MOO method is performed for optimizing the forearm design. The numerical model of the forearm structure is displayed in Fig. 15. In this optimization design problem, the maximum stress and the weight of the forearm structure are adopted as two optimization objectives. The maximum displacement of the forearm structure in the vertical direction is considered as the constraint. Four thickness parameters of the forearm structure are identified as the design variables. The material properties of the forearm structure are as follows: the density is 7.85g/cm^3 , the Young's modulus is 200Gpa, the Poisson's ratio is 0.2, and the permissible maximum stress is 230 MPa. Therefore, the optimization design problem can be described as follows:

$$\begin{aligned} \min_{\mathbf{X}} (P(\mathbf{X}), M(\mathbf{X})) \text{ s.t. } D(\mathbf{X}) \leq 25\text{mm} \\ = (X_1, X_2, X_3, X_4)^T \quad 8\text{mm} \leq X_1, X_2, X_3, X_4 \leq 14\text{mm} \quad (18) \end{aligned}$$

where $P(\mathbf{X})$ stands for the maximum stress of the forearm structure and $M(\mathbf{X})$ is the total weight of the forearm. $D(\mathbf{X})$ is the maximum displacement of the forearm in the vertical direction. \mathbf{X} stands for the design vector: X_1 represents the thickness of the girder web, X_2 is the thickness of the diagonal beam, X_3 is the thickness of the flange plate on the cross beam, and X_4 stands for the thickness of the flange plate on the girder.

In the optimization process, the allowable error δ is set to 0.05. The μ MOGA and local-densifying approximation method are also used to solve the Pareto optimal set. The preset parameters for μ MOGA are as follows: the maximum generation is 200, and the population size and the probability of crossover are 5.0 and 0.5. The approximation models of the objective functions $P(\mathbf{X})$ and $M(\mathbf{X})$ and constraint $D(\mathbf{X})$ are constructed by using thirty initial samples which are generated by the LHD. Based on the proposed RSPAM ($M = 5$), The optimal shape parameters of approximation models $\tilde{P}(\mathbf{X})$, $\tilde{M}(\mathbf{X})$, and $\tilde{D}(\mathbf{X})$ are obtained by RSPAM, which are 0.1020, 0.1295, and 0.6390, respectively. The corresponding approximation models are constructed based on these samples and shape parameters. Under the help of the present method, the iterative process and the optimization results are illustrated in Fig. 16 and the count of samples in iterative steps are given in Table 12. Summing up the above results, the final Pareto optimal set satisfying the allowable error can be obtained in step 2, in which the maximal error of the objective functions and constraints is 1.08%. Therefore, eleven solutions are

Fig. 16 The iterative process and optimization results (engineering example B)



obtained as listed in Table 13. The engineer's different attention to the optimization objectives will determine the choice of the Pareto solution. If the maximum stress of the forearm structure is the primary concern, the No.1 solution could be selected; if the minimal weight of the forearm structure is the most important, the No.2 solution could be selected. Depending on the optimization results, the engineers could choose the appropriate optimization solution to ensure the safety of the forearm structure.

5 Conclusion

This paper provides an efficient multi-objective optimization (MOO) method based on the adaptive approximation model. In this method, the approximation models based on radial basis function (RBF) is used to instead of the actual objective functions and constraint functions of the MOO problem. For improving the prediction ability and accuracy of the approximation model, the reverse shape parameter analysis method (RSPAM) is proposed. By using the RSPAM, the equation for calculating the shape parameter is established based on initial samples and the optimal shape parameter is solved according to the error criterion. Compared to the traditional approximation model technology, the optimal shape parameter can be obtained effectively without additional sampling, which effectively reduces the model error caused by the operator's experience. Moreover, the local-densifying approximation method is employed to densify more samples into the local area where the Pareto optimal set of objective functions and their corresponding constraint functions. Because the prediction ability and accuracy of approximation model in local area we concerned is guaranteed, the Pareto optimal set can be further improved. The computational results of two numerical examples demonstrate the outstanding performance of the proposed method in solving the optimization solutions. This method is also performed for the optimization design problems of the gear transmission structure and the forearm of the bucket wheel stacker-reclaimer. The satisfactory optimization results further demonstrate the suitability of the proposed method in

practical applications. It is noteworthy that the accurate optimization results are ensured by the RSPAM and local-densifying approximation method. Additionally, when the high-dimensional and strong simulation models are involved, the more initial samples should be adopted to construct the RBF approximation model and more local-densifying iterations should be processed to obtain the accurate optimization solutions. Hence, how to greatly improve the abovementioned problems for better efficiency has been included in our future work.

Acknowledgments The authors would also like to thank anonymous reviewers for their valuable comments.

Funding This work is supported by the National Natural Science Foundation of China (Grant No.51775057, 51875049), the Scientific Research Fund of Hunan Provincial Education Department (No.16B014), and Open Fund of Engineering Research Center of Catastrophic Prophylaxis and Treatment of Road & Traffic Safety of Ministry of Education (kfj170401).

Compliance with ethical standards

The conflict of interest The authors declare that they have no conflict of interest.

Replication of results The results presented in this article can be replicated by implementing the data structures and algorithms presented in this article. Because the codes of algorithms are not open source, the authors wish to withhold the code for commercialization purposes.

References

- Amouzgar K, Strömberg N (2017) Radial basis functions as surrogate models with a priori bias in comparison with a posteriori bias. *Struct Multidiscip Optim* 55(4):1453–1469. <https://doi.org/10.1007/s00158-016-1569-0>
- Bu JG, Lan XD, Zhou M, Lv KX (2018) Performance optimization of flywheel motor by using NSGA-2 and AKMMP. *IEEE Trans Magn* 54(6):8103707. <https://doi.org/10.1109/TMAG.2017.2784401>
- Bui VH, Hussain A, Lee WG, Kim HM (2019) Multi-objective optimization for determining trade-off between output power and power fluctuations in wind farm system. *Energies* 12(22):4242. <https://doi.org/10.3390/en12224242>

- Cheng GH, Younis A, Haji Hajikolaie K, Gary WG (2015) Trust region based mode pursuing sampling method for global optimization of high dimensional design problems. *J Mech Des* 137(2):021407. <https://doi.org/10.1115/1.4029219>
- Choi BC, Cho S, Kim CW (2018) Kriging model based optimization of MacPherson strut suspension for minimizing side load using flexible multi-body dynamics. *Int J Precis Eng Manuf* 19(6):873–879. <https://doi.org/10.1007/s12541-018-0103-2>
- Fang JG, Gao YK, Sun GY, Zhang YT, Li Q (2014) Crashworthiness design of foam-filled bitubal structures with uncertainty. *Int J Non Linear Mech* 67:120–132. <https://doi.org/10.1016/j.ijnonlinmec.2014.08.005>
- Fasshauer GE, Zhang JG (2007) On choosing “optimal” shape parameters for RBF approximation. *Numer Algorithms* 45:345–368. <https://doi.org/10.1007/s11075-007-9072-8>
- Fornberg B, Piret C (2008) On choosing a radial basis function and a shape parameter when solving a convective PDE on a sphere. *J Comput Phys* 227(5):2758–2780. <https://doi.org/10.1016/j.jcp.2007.11.016>
- Garud SS, Karimi IA, Kraft M (2017) Smart sampling algorithm for surrogate model development. *Comput Chem Eng* 96:103–114. <https://doi.org/10.1016/j.compchemeng.2016.10.006>
- Hu L, Hu XT, Wang J, Kuang AW, Hao W, Lin M (2020) Casualty risk of e-bike rider struck by passenger vehicle using China in-depth accident data. *Traffic Inj Prev* 21(4):283–287. <https://doi.org/10.1080/15389588.2020.1747614>
- Husslage B, Rennen G, Dam E, Hertog D (2011) Space-filling Latin hypercube designs for computer experiments. *Optim Eng* 12:611–630. <https://doi.org/10.1007/s11081-010-9129-8>
- Jang BS, Ko DE, Suh YS, Yang YS (2009) Adaptive approximation in multi-objective optimization for full stochastic fatigue design problem. *Mar Struct* 22(3):610–632. <https://doi.org/10.1016/j.marstruc.2008.11.001>
- Jaouadi Z, Abbas T, Morgenthal G, Lahmer T (2020) Single and multi-objective shape optimization of streamlined bridge decks. *Struct Multidiscip Optim* 61(4):1495–1514. <https://doi.org/10.1007/s00158-019-02431-3>
- Joseph VR, Gul E, Ba S (2015) Maximum projection designs for computer experiments. *Biometrika* 102(2):371–380. <https://doi.org/10.1093/biomet/asv002>
- Kiani M, Yildiz AR (2016) A comparative study of non-traditional methods for vehicle crashworthiness and NVH optimization. *Arch Comput Meth Eng* 23(4):723–734. <https://doi.org/10.1007/s11831-015-9155-y>
- Koupaei JA, Firouznia M, Hosseini SMM (2018) Finding a good shape parameter of RBF to solve PDEs based on the particle swarm optimization algorithm. *Alex Eng J* 57(4):3641–3652. <https://doi.org/10.1016/j.aej.2017.11.024>
- Lee YB, Oh S, Choi DH (2008) Design optimization using support vector regression. *J Mech Sci Technol* 22(2):213–220. <https://doi.org/10.1007/s12206-007-1027-4>
- Liew KM, Chen XL, Reddy JN (2004) Mesh-free radial basis function method for buckling analysis of non-uniformly loaded arbitrarily shaped shear deformable plates. *Comput Method Appl Mech Eng* 193(3–5):205–224. <https://doi.org/10.1016/j.cma.2003.10.002>
- Liu GP, Han X, Jiang C (2012) An efficient multi-objective optimization approach based on the micro genetic algorithm and its application. *Int J Mech Mater Des* 8(1):37–49. <https://doi.org/10.1007/s10999-011-9174-2>
- Liu J, Sun XS, Han X, Jiang C, Yu DJ (2015) Dynamic load identification for stochastic structures based on Gegenbauer polynomial approximation and regularization method. *Mech Syst Signal Process* 56–57: 35–54. <https://doi.org/10.1016/j.ymssp.2014.10.008>
- Liu X, Kuang ZX, Yin LR, Hu L (2017a) Structural reliability analysis based on probability and probability box hybrid model. *Struct Saf* 68:73–84. <https://doi.org/10.1016/j.strusafe.2017.06.002>
- Liu X, Yin LR, Hu L, Zhang ZY (2017b) An efficient reliability analysis approach for structure based on probability and probability box models. *Struct Multidiscip Optim* 56(1):167–181. <https://doi.org/10.1007/s00158-017-1659-7>
- Liu X, Fu Q, Ye NH, Yin LR (2019a) The multi-objective reliability-based design optimization for structure based on probability and ellipsoidal convex hybrid model. *Struct Saf* 77:48–56. <https://doi.org/10.1016/j.strusafe.2018.11.004>
- Liu X, Wang XY, Sun L, Zhou ZH (2019b) An efficient multi-objective optimization method for uncertain structures based on ellipsoidal convex model. *Struct Multidiscip Optim* 59(6):2189–2203. <https://doi.org/10.1007/s00158-018-2185-y>
- Liu X, Wang XY, Xie J, Li BT (2020) Construction of probability box model based on maximum entropy principle and corresponding hybrid reliability analysis approach. *Struct Multidiscip Optim* 61(2): 599–617. <https://doi.org/10.1007/s00158-019-02382-9>
- Long T, Li XL, Huang B, Jiang ML (2016) Aerodynamic and stealthy performance optimization of airfoil based on adaptive surrogate model. *J Mech Eng* 52(22):101–111. <https://doi.org/10.3901/JME.2016.22.101>
- Lu YM, Roychowdhury V (2008) Parallel randomized sampling for support vector machine (SVM) and support vector regression (SVR). *Knowl Inf Syst* 14(2):233–247. <https://doi.org/10.1007/s10115-007-0082-6>
- Manshadi MD, Jamalinasab M (2017) Optimizing a two-element wing model with morphing flap by means of the response surface method. *Iran J Sci Tech Trans Mech Eng* 41(4):343–352. <https://doi.org/10.1007/s40997-016-0067-8>
- Omkar SN, Senthilnath J, Khandelwal R, Narayana Naik G, Gopalakrishnan S (2011) Artificial bee colony (ABC) for multi-objective design optimization of composite structures. *Appl Soft Comput* 11(1):489–499. <https://doi.org/10.1016/j.asoc.2009.12.008>
- Park JS (1994) Optimal Latin-hypercube designs for computer experiments. *J Stat Plann Inference* 39(1):95–111. [https://doi.org/10.1016/0378-3758\(94\)90115-5](https://doi.org/10.1016/0378-3758(94)90115-5)
- Peng X, Liu ZY, Xu XQ, Li JQ, Qiu C, Jiang SF (2018) Nonparametric uncertainty representation method with different insufficient data from two sources. *Struct Multidiscip Optim* 58(5):1947–1960. <https://doi.org/10.1007/s00158-018-2003-6>
- Posteljnik Z, Stupar S, Svorcan J, Peković O, Ivanov T (2016) Multi-objective design optimization strategies for small-scale vertical-axis wind turbines. *Struct Multidiscip Optim* 53(2):277–290. <https://doi.org/10.1007/s00158-015-1329-6>
- Sarra SA, Sturgill D (2009) A random variable shape parameter strategy for radial basis function approximation methods. *Eng Anal Bound Elem* 33(11):1239–1245. <https://doi.org/10.1016/j.enganabound.2009.07.003>
- Stolunov V, Nair PB (2018) Sparse radial basis function approximation with spatially variable shape parameters. *Appl Math Comput* 330: 170–184. <https://doi.org/10.1016/j.amc.2018.02.001>
- Tian Y, Cheng R, Zhang XY, Cheng F, Jin YC (2018) An indicator-based multiobjective evolutionary algorithm with reference point adaptation for better versatility. *IEEE Trans Evol Comput* 22(4):609–622. <https://doi.org/10.1109/TEVC.2017.2749619>
- Wang G (2003) Adaptive response surface method using inherited Latin hypercube design points. *J Mech Des* 125(2):210–220. <https://doi.org/10.1115/1.1561044>
- Wang G, Dong ZM, Aitchison P (2001) Adaptive response surface method - a global optimization scheme for approximation-based design problems. *Eng Optim* 33(6):707–733. <https://doi.org/10.1080/03052150108940940>
- Wang XD, Hirsch C, Kang S, Lacor C (2011) Multi-objective optimization of turbomachinery using improved NSGA-II and approximation model. *Comput Method Appl Mech Eng* 200(9–12):883–895. <https://doi.org/10.1016/j.cma.2010.11.014>

- Yang BS, Yeun YS, Ruy WS (2002) Managing approximation models in multiobjective optimization. *Struct Multidiscip Optim* 24:141–156. <https://doi.org/10.1007/s00158-002-0224-0>
- Zarchi M, Attaran B (2019) Improved design of an active landing gear for a passenger aircraft using multi-objective optimization technique. *Struct Multidiscip Optim* 59(5):1813–1833. <https://doi.org/10.1007/s00158-018-2135-8>
- Zhang DQ, Han X, Jiang C, Liu J, Li Q (2017) Time-dependent reliability analysis through response surface method. *J Mech Des* 139(4): 041404. <https://doi.org/10.1115/1.4035860>
- Zhang DQ, Zhang N, Ye N, Fang JG, Han X (2020) Hybrid learning algorithm of radial basis function networks for reliability analysis. *IEEE Trans Reliab*. <https://doi.org/10.1109/TR.2020.3001232>

Publisher's note Springer Nature remains neutral with regard to jurisdictional claims in published maps and institutional affiliations.